ELSEVIER

Thermochimica Acta 399 (2003) 43–55

thermochimica acta

www.elsevier.com/locate/tca

Glass transitions in frozen sucrose solutions are influenced by solute inclusions within ice crystals

H.D. Goff*, E. Verespej, D. Jermann

Department of Food Science, University of Guelph, Guelph, ON, Canada N1G 2W1

Received 28 June 2002; received in revised form 17 July 2002; accepted 17 July 2002

Abstract

Modulated temperature–differential scanning calorimetry (MT–DSC) and microscopy were used to examine the glass transition behavior of frozen 40% sucrose solutions under various freezing conditions, and to correlate this behavior to observed microstructural differences in the samples. Freezing procedures that resulted in deep undercooling followed by rapid nucleation led to two glass-like transitions upon warming. Micrographs of the structure resulting from this freezing process revealed the presence of sucrose inclusions within the ice crystals. It is believed that the lower transition represents the glass transition of the bulk phase, T_g' after annealing to approach maximal freeze-concentration, while the second, warmer transition is related to the presence of the solute inclusions. However, maturation of these crystals leading to a pure crystalline phase and a homogeneous bulk phase led to a change of the warmer baseline shift during warming from a glass-like transition to a non-reversing transition. Thus, the freezing procedure dictates the structure within the sample, which then dictates thermal behavior.

Keywords: Glass transition; Sucrose solutions; T_g'; Freeze-concentration; Solute inclusions

1. Introduction

Many frozen foods contain high sugar contents (e.g. fruits, dessert products, ice cream). The presence of sugar depresses the initial freezing point and, due to subsequent freeze-concentration of the sugars, results in a temperature-dependent equilibrium between the ice crystals and the unfrozen solution surrounding them [1]. At sufficiently low temperature, this freeze-concentrated unfrozen phase reaches sufficient viscosity to become glassy. Many studies have been conducted using sucrose solutions to model these frozen foods [2–7]. Although the state diagram has been modeled and published by many people [8–11], one difficulty has always been reconciling experimental data with the state diagram [12]. On warming a maximally freeze-concentrated sugar solution, one that has been properly annealed at $T > T_g$ to promote maximal freeze-concentration, in a differential scanning calorimetry (DSC), two baseline shifts in the heat flow curve are evident [2,3,6,10,11]. Assigning these two events on the state diagram has been controversial [11–13]. The most widely accepted belief at present seems to be that the lower temperature transition (Transition 1, "Tr_1"), at around $-40\,^{\circ}C$ in properly annealed sucrose solutions, is T_g', the T_g of the maximally freeze-concentrated glass [8,9]. The warmer temperature transition (Transition 2, "Tr_2"),

* Corresponding author. Tel.: +1-519-824-4120x3878; fax: +1-519-824-6631.
E-mail address: dgoff@uoguelph.ca (H.D. Goff).

0040-6031/02/$ – see front matter
PII: S0040-6031(02)00399-4

at around −32 °C, represents the onset of melting of ice crystals [10,11,14,15]. This warmer temperature transition is often denoted T'_m, and results from delayed melting of ice into the highly viscous unfrozen phase [10,11,14,15].

Recent research from our laboratory, using modulated temperature (MT)–DSC, has shown that freezing protocol has a large influence on the thermal behavior of these transitions [16]. In quiescently frozen and annealed solutions, both transitions exhibited glass transition-like behavior. However, after sucrose solutions had been dynamically frozen in a scraped-surface heat exchanger and subsequently hardened, their thermal behavior was much different. Although still present in the total heat flow curve, the warmer temperature transition, Tr_2, had completely disappeared from the complex heat capacity (C_p^*) curve, where reversing events such as glass transitions should be evident. The above results implied that the Tr_2 no longer exhibited glass transition-like behavior after dynamic freezing. The Tr_2 in the C_p^* curve was also found to disappear with repeated temperature cycling of quiescently frozen samples at −15±5 °C, while the endotherm in the non-reversing curve became more of a baseline shift. This implied that the quiescently frozen sample took on characteristics typical of the dynamically-frozen sample after temperature cycling. With storage of quiescent-frozen samples at −30 °C, a complete loss of Tr_2 in the C_p^* curve was seen within 3 weeks. The non-reversing curve showed the baseline shift at Tr_2 after 3 weeks, characteristic of the dynamically-frozen samples. This again implied that storage of frozen samples at $T > T_g$ was sufficient to convert the thermal behavior of these samples from that of their original quiescent condition to one similar to that seen in the dynamically-frozen samples. The dynamically-frozen samples showed no change in thermal behavior as a result of temperature cycling. Thus, the nature of Tr_2, the higher temperature relaxation, was changed by either dynamic freezing, or by temperature cycling of quiescently frozen samples, or by storing quiescently frozen samples at $T > Tr_2$.

Microstructural differences revealed that ice crystal size or surface area may have had an effect, but so too did ice crystal morphology [16]. Quiescent freezing resulted in considerable undercooling, followed by rapid nucleation and very small, dendritic, crystals. The glass transition-like nature of Tr_2 may have resulted from the formation of a sucrose-rich, unequilibrated phase trapped around or within the rapidly nucleated ice crystals, and/or solute inclusions within the crystals themselves. Such a phase may have arisen from a concentration gradient and limited diffusion at the crystal interface. This phase relaxed at a higher temperature than did the bulk unfrozen phase, resulting in the two-step glass transition. When this phase disappeared, from maturation or perfection of the ice crystals or equilibration of the unfrozen phase, the transition seen at Tr_2 in the total heat flow curve lost its glass transition-like characteristics, and then appeared to have been solely due to the onset of delayed melting. It was proposed that heterogeneity exists in the unfrozen phase of quiescently frozen solutions, leading to another phase more concentrated in sucrose than the bulk phase. This sucrose phase would only be formed in quiescent systems, as a result of rapid nucleation. It is possible that the diffusion of water to the surface of a crystal at low temperatures, from the neighborhood of the crystal, was not compensated by diffusion from the bulk phase. This would have produced a concentrated, non-equilibrated phase around the crystal, which would be detected as a glass transition in the reversing component (at Tr_2) during warming of the frozen solution in the MT–DSC. Such a phase would disappear after temperature cycling, because of the mobility of the unfrozen phase at temperatures higher than T'_g, leading to perfection of the surfaces of crystals and homogeneity in the unfrozen phase. In dynamic systems, the nature of the crystallization process would have prevented its formation at a detectable level.

Three recent papers have used MT–DSC to look at the glass transition in frozen sucrose solutions [13,17,18]. Aubuchon et al. [13] followed a “slow freeze and anneal” method and showed the same results as those of our quiescently frozen samples. They concluded, also from quasi-isothermal experimental results, that Tr_2 is a glass transition (or at least appears glass transition-like). Knopp et al. [18] cooled their sucrose solutions to −25 °C, then warmed to −10 °C and held for 20 min, then cooled to $T < T_g$ and rewarmed. They showed the same results as those from the dynamically-frozen samples, the quiescently frozen and temperature cycled samples, and the stored samples, viz. no Tr_2 in the C_p^* curve, although it was seen in the total heat flow curve. They concluded that

Tr_2 was not a glass transition, but the onset of melting. Thus, it appears that the freezing protocol has a major impact on the nature of Tr_2.

The objective of this experiment is to use both MT–DSC and microscopical techniques to further examine the glass transition behavior of the Tr_2 under various freezing conditions, and to correlate this behavior to observed microstructural differences in the samples.

2. Experimental

DSC analyses: Sucrose solutions (40 or 82%) were prepared with reagent grade sucrose (Fisher, Toronto, Canada) by heating the solution to 80 °C, adding back evaporated water, and storing at 4 (40%) or 0 °C (82%) for several hours before use. A MT–DSC (Q1000, TA Instruments, New Castle, DE) was used for thermal evaluation. T_0 calibration was performed with sapphire, heat flow calibration was performed with gallium, temperature calibration was performed with gallium and indium, and heat capacity calibration was performed with sapphire. Nitrogen (300 ml/min) was used as a purge gas. A heat-only modulation, amplitude of ±0.318 °C, period of 60 s was used in all experiments (preliminary work had optimized modulation conditions and ramp rates). Hermetically-sealed alod-al pans (TA Instruments) were used; sample size was approximately 10 mg.

A two-cycle protocol was used for 40% solutions, as follows: equilibrate at 25 °C, modulation on, isothermal 5 min, ramp 2 °C/min to −80 °C (first cool), modulation off, anneal by heating at 5 °C/min to −35 °C, holding 60 min and then back to −80 °C at 5 °C/min, modulation on, isothermal 5 min, ramp 2 °C/min to −5 °C (first warm), ramp 2 °C/min to −80 °C (second cool), modulation off, anneal again as above, modulation on, isothermal 5 min, ramp 2 °C/min to 5 °C (second warm). Nine runs of each protocol were made and results were averaged. For 82% sucrose solutions, the procedure above was used for the first cool and first warm only. Six runs of each protocol were made and results were averaged. Another set of experiments was done utilizing a tempering protocol, rather than the two-cycle protocol. In these experiments, the method was as follows: equilibrate at 25 °C, ramp 2 °C/min to −25 °C, ramp 2 °C/min to −10 °C, isothermal 20 min, ramp 2 °C/min to −80 °C, anneal by heating at 2 °C/min to −35 °C, holding for 60 min and then back to −80 °C at 2 °C/min, modulation on, isothermal 5 min, ramp 2 °C/min to 5 °C. Duplicate runs of each protocol were made and results were averaged.

Microscopy: Microstructure was evaluated by cold-stage light microscopy and cryo-scanning electron microscopy (SEM). For light microscopy, a Linkam LTS350 temperature controlled stage, attached to a TMS93 controller with liquid nitrogen pump (Linkam Scientific Instruments, Tadworth, Surrey, UK), was used on an Olympus BH microscope. A drop of 40% sucrose solution was placed on a microscope slide under a cover slip. The cold-stage program was similar to the two-cycle DSC protocol above, as follows: ramp 2 °C/min to −60 °C (first cool), ramp 2 °C/min to −7 °C (first warm), ramp 2 °C/min to −60 °C (second cool), ramp 2 °C/min to 5 °C (second warm). Digital images were collected at 5 °C intervals throughout the experiment. The experiment was repeated three times.

For SEM, 40% sucrose solutions were frozen in the DSC in unsealed aluminum pans according to the following method: equilibrate at 25 °C, ramp 2 °C/min to −60 °C, ramp 2 °C/min to −35 °C and remove (for warm 1), and equilibrate at 25 °C, ramp 2 °C/min to −60 °C, ramp 2 °C/min to −7 °C, ramp 2 °C/min to −60 °C, ramp 2 °C/min to −35 °C and remove (for warm 2). The tempering method above was also used, as follows: equilibrate at 25 °C, ramp 2 °C/min to −25 °C, ramp 2 °C/min to −10 °C, isothermal 20 min, ramp 2 °C/min to −60 °C, ramp 2 °C/min to −35 °C and remove. Samples after removal from the DSC were immediately immersed in liquid nitrogen (−150°C), and transferred to the cryo-SEM (Hitachi S-570 SEM, Hitachi Ltd., Tokyo, Japan). The sample stub for cryo-SEM consisted of a copper base with a gorged area along the stub and two spring loaded supports [19,20]. Two specimens (∼2–3 mm cubes) of each sample were placed in the stub while immersed in liquid nitrogen slush. The stub was then transferred under vacuum (1×10^{-2} Torr) to the preparation chamber (Emscope SP2000A Sputter-Cryo Cryogenic preparation System, Emscope Ltd., Kent, UK) using the transfer device. Specimens were fractured using the blade in the preparation chamber and transferred to the cold stage of the SEM for

sublimation (−80 °C). An average sublimation time was determined so as to allow clear differentiation of the crystal sockets (∼20–25 min). After etching, the stubs were transferred back to the preparation chamber for gold sputter-coating (2.5 min). Specimens were viewed at 10 kV accelerating voltage with an objective lens aperture of 50 μm. Digital images were collected using the Voyager Acquisition System (Noran Instruments, Middleton, WI). The experiment was repeated three times with at least 20 images collected at different magnifications from each replicate.

3. Results

The thermograms from the TA Q1000 DSC were very repeatable with different replications. The average standard error of the mean for temperatures in the total heat flow curves was 0.13 for Tr_1 and Tr_2, cooling and warming, on 40% sucrose solutions and 0.65, cooling and warming, on 82% sucrose solutions. In the reversing heat flow curve, the average standard error of the mean for temperatures was 0.11 for Tr_1 and 0.28 for Tr_2 on 40% sucrose solutions and 0.65 for 82% sucrose solutions.

Figs. 1 and 2 present the total heat flow curves for both cooling and warming cycles of the two-cycle protocol. In the first cool, nucleation typically occurred between −18 and −20 °C. A baseline shift in the total heat flow curve at Tr_2 occurred in the first cool, but not in the second cool, whereas smaller baseline shifts were evident in both cooling cycles at Tr_1 (Fig. 1). The height of the Tr_1 transition was slightly larger and the temperature was lower in the second cool compared to the first (Table 1). After annealing, the Tr_1 was exactly the same, both temperature and height, in the first and second warming cycles (Fig. 2 and Table 1). Tr_2 transitions were evident in both warming cycles and were 3–4 times larger in height than the Tr_1 transitions. Tr_2 in the second warm cycle was shifted warmer by 2.5 °C than in the first warming cycle. Tr_2 in the first warm showed an overshoot, typical of an enthalpic relaxation, before moving into the melting endotherm, whereas Tr_2 in the second warm did not (Fig. 2). This makes its height appear larger (Table 1) and makes it difficult to characterize the transition quantitatively. After the complex relaxation through both Tr_1 and Tr_2,

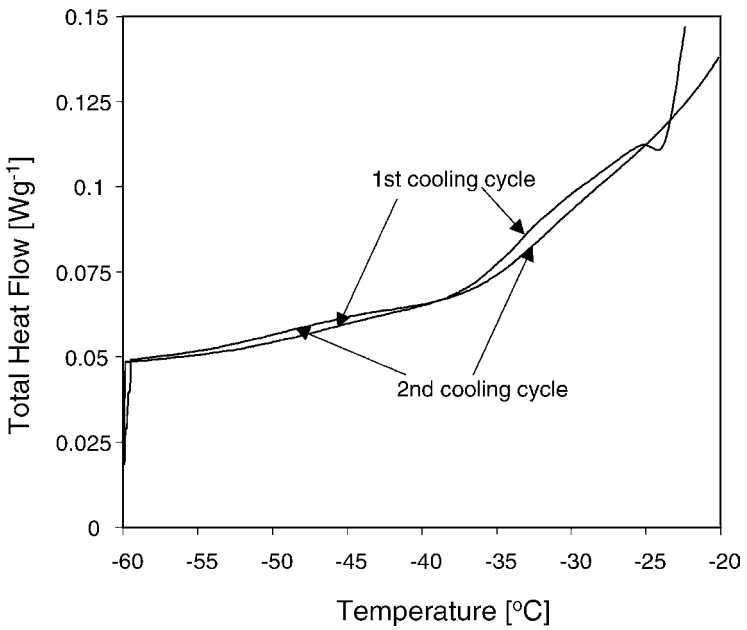

Fig. 1. Total heat flow as a function of temperature for a 40% sucrose solution that was cooled to −80 °C at 2 °C/min (first cooling cycle), annealed at −35 °C, recooled to −80 °C, warmed at 2 °C/min to −5 °C, and recooled at 2 °C/min to −80 °C (second cooling cycle).

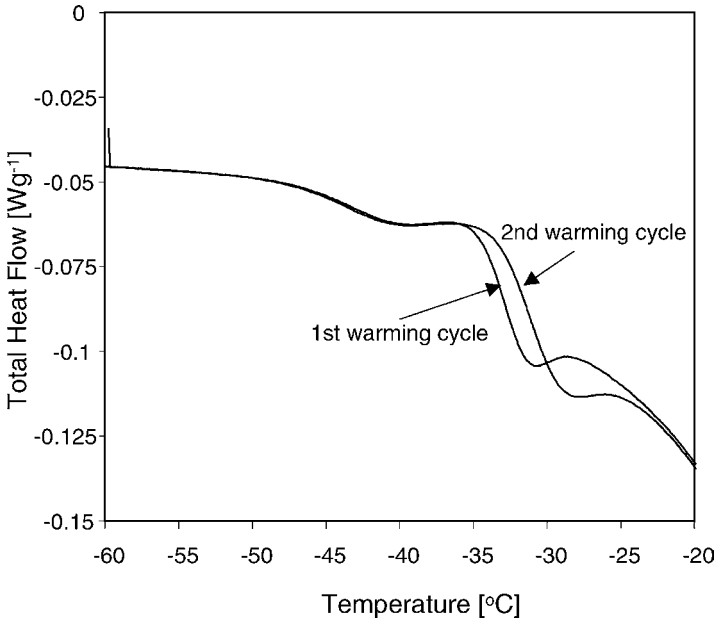

Fig. 2. Total heat flow as a function of temperature for a 40% sucrose solution that was cooled to −80 °C at 2 °C/min, annealed at −35 °C, recooled to −80 °C, warmed at 2 °C/min to −5 °C (first warming cycle), recooled at 2 °C/min to −80 °C, annealed at −35 °C, recooled to −80 °C, and warmed at 2 °C/min to 5 °C (second warming cycle).

the melting endotherm onsets were exactly the same in both warming cycles (Fig. 2).

MT–DSC was used to deconvolute the Tr_1 and Tr_2 transitions into reversing (heat capacity related) and non-reversing (total minus reversing) signals. The reversing ("complex") heat capacity is shown in Fig. 3 for all four temperature sweeps. The Tr_2 transition was evident as a reversing event in the first cooling and first warming cycles. The heights and temperatures for this transition were similar in both cycles (Table 2). However, the Tr_2 did not appear in the second cooling or warming cycles (Fig. 3). The Tr_1 transitions were all

Table 1
Characteristics of the two transitions in the total heat flow curve of frozen sucrose solutions

	Tr_1					Tr_2				
	Onset[a] (°C)	Midpoint (°C)	End[a] (°C)	Height (J/(g °C))	Width (°C)	Onset[a] (°C)	Midpoint (°C)	End[a] (°C)	Height (J/(g °C))	Width (°C)
First cool	−51.6	−45.9	−44.5	0.0084	7.1	−35.8	−33.4	−32.1	0.019	3.7
First warm	−47.4	−43.4	−42.1	0.011	5.3	−34.4	−33.0	−32.5	0.030	1.9
Second cool	−54.4	−49.3	−45.6	0.010	8.8	−35.3	–	–	–	–
Second warm	−47.5	−43.5	−42.1	0.011	5.4	−33.2	−31.3	−29.8	0.043	3.4
First warm[b]	−49.8	−46.8	−45.3	0.0095	4.5	−34.1	−32.2	−30.4	0.042	3.7
82% cool	−41.5	−36.1	−31.7	0.018	9.8	–	–	–	–	–
82% warm	−38.6	−34.8	−33.6	0.018	5.0	–	–	–	–	–

40% sucrose, unless noted otherwise; see Section 2 for temperature profiles of the samples.

[a] Onset and end represent the lowest and highest temperature values, respectively, regardless of the direction of the scan.

[b] From the tempering method (see Section 2 for description).

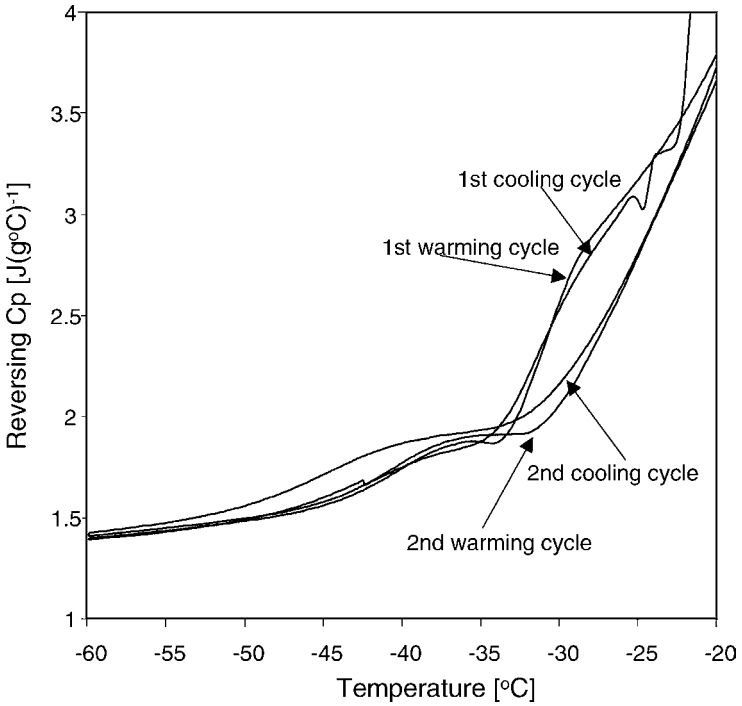

Fig. 3. Reversing heat capacity as a function of temperature for the two cooling and warming cycles described in Figs. 1 and 2.

similar in temperature and size, except that the temperature was shifted about 4 °C lower in the second cool (Table 2).

Fig. 4 shows the non-reversing heat flow associated with the two warming cycles. Both warming cycles show a small endotherm associated with Tr_1, which was exactly the same in temperature and height in both cases. At Tr_2, both warming cycles also showed small transitions, but the nature of them was different in each case. In the second warm, the onset was at a slightly higher temperature, it was slightly larger in height, and it did not return to the baseline as an endotherm.

Table 2
Characteristics of the two transitions in the reversing heat flow curve of frozen sucrose solutions

	Tr_1					Tr_2				
	Onset[a] (°C)	Midpoint (°C)	End[a] (°C)	Height (J/(g °C))	Width (°C)	Onset[a] (°C)	Midpoint (°C)	End[a] (°C)	Height (J/(g °C))	Width (°C)
First cool	−46.7	−41.8	−39.4	0.0095	7.5	−33.3	−31.0	−29.1	0.025	4.2
First warm	−44.5	−40.3	−38.2	0.0097	6.3	−32.2	−31.1	−29.3	0.025	2.8
Second cool	−49.5	−44.5	−40.8	0.010	8.7	–	–	–	–	–
Second warm	−44.6	−40.4	−37.9	0.010	6.7	–	–	–	–	–
First warm[b]	−47.1	−43.7	−40.3	0.010	6.7	–	–	–	–	–
82% cool	−37.5	−31.9	−27.6	0.020	10.0	–	–	–	–	–
82% warm	−35.7	−31.4	−27.6	0.021	8.1	–	–	–	–	–

40% sucrose, unless noted otherwise; see Section 2 for temperature profiles of the samples.

[a] Onset and end represent the lowest and highest temperature values, respectively, regardless of the direction of the scan.

[b] From the tempering method (see Section 2 for description).

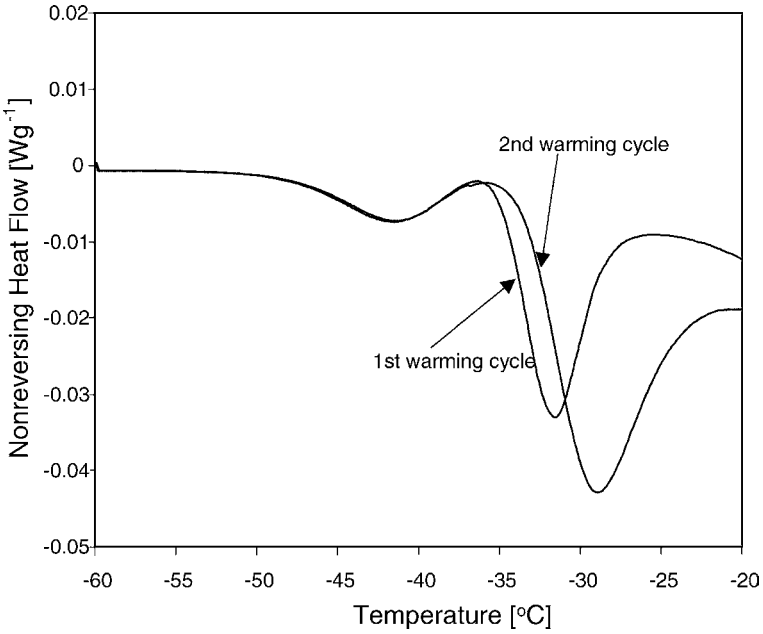

Fig. 4. Non-reversing heat flow as a function of temperature for the two warming cycles described in Fig. 2.

Thus, it is obvious that the baseline shift in the total heat flow curve at Tr_2 in the second warm came from the non-reversing curve, not the reversing curve.

Images from light microscopy of the structure throughout this process illustrated the change in ice crystal morphology from the first warm to the second warm (Fig. 5). At the resolution of the light microscope (400×), nucleation during the first cool at about −20 °C resulted in a cloud of crystals too small to be detectable (as seen by the darkening in Fig. 5). It is likely that this microstructure led to a heterogeneous distribution of sucrose and ice crystals, which would lead to a complex relaxation of the glass. However, once the crystals were ripened through the first warm and second cool, they became discrete and easily resolved. Crystal morphology and unfrozen phase structure were also examined by cryo-SEM (Fig. 6). The ice crystals at −35 °C during the first warm were very dendritic (Fig. 6A). There was evidence of considerable amorphous sucrose within the crystals themselves, as evident from the material left behind after sublimation (Fig. 6B). However, the microstructure at −35 °C during the second warm showed a much more homogeneous distribution of unfrozen phase surrounding discrete, rounded crystals (Fig. 6C). In this case, no evidence of amorphous sucrose was seen in any of the ice crystal sockets (Fig. 6D).

Knopp et al. [18] cooled sucrose solutions to −25 °C, then warmed to −10 °C and held 20 min, then cooled to $T < T_g$ and rewarmed. They showed the same results as ours in the second warm above, viz. no Tr_2 in the reversing (complex) heat capacity curve, although it was seen in the total heat flow curve. We repeated their protocol (referred to as the "tempering" method) and found similar qualitative results. The Tr_1 was shifted about 3 °C lower in total heat flow and reversing heat capacity while the Tr_2 was shifted 1 °C lower in total heat flow. Both the second warm from the two-cycle method above and the first warm from this tempering method were similar in height at the Tr_1 and at the Tr_2 (Tables 1 and 2). Cryo-SEM of the structure at −35 °C from this tempering protocol showed similar structure to the second warm above, viz. no amorphous sucrose inclusions within the ice crystals (Fig. 7).

It was also informative to examine by MT–DSC the thermal behavior of a solution of 82% sucrose, as at this concentration no ice forms, and this is considered

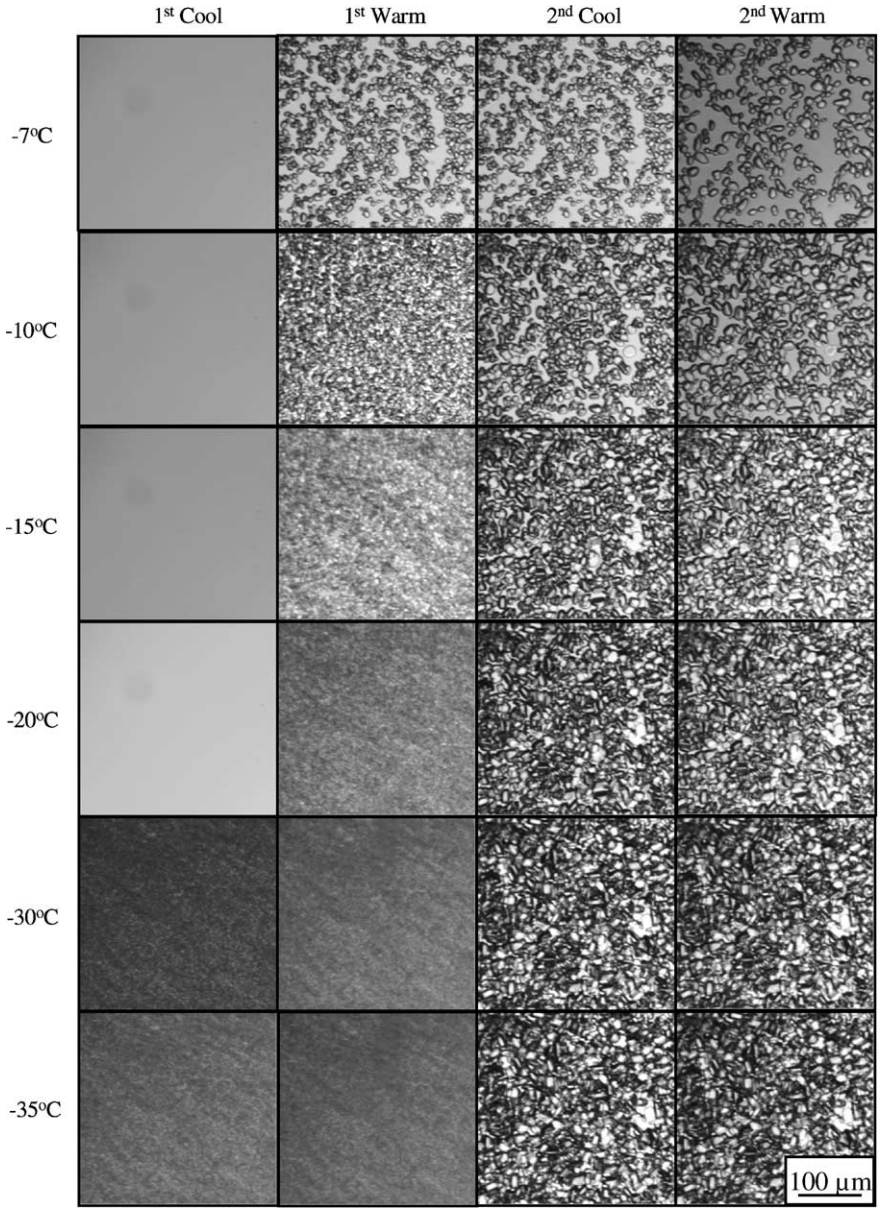

Fig. 5. Images of 40% sucrose solutions on a cold stage of a light microscope, following the same temperature regime as the thermograms in Figs. 1 and 2. The solution was first cooled to −60 °C (left column, from top to bottom; nucleation occurred at −21 °C), then warmed to −5 °C (second column from left, bottom to top), cooled again to −60 °C (second column from right, top to bottom), and finally warmed from −60 to 5 °C (right column, bottom to top). Representative images at −7, −10, −15, −20, −30 and −35 °C are shown.

to be the maximal concentration of sucrose in the unfrozen phase at T_g' [21]. As seen in Fig. 8, only one reversing heat capacity transition is seen during the warming of such systems, accompanied with a small non-reversing endotherm. The transition in the total and in the reversing heat flow was much broader in width and larger than that seen in the 40% sucrose solution, with a height nearly double that seen in Tr_1

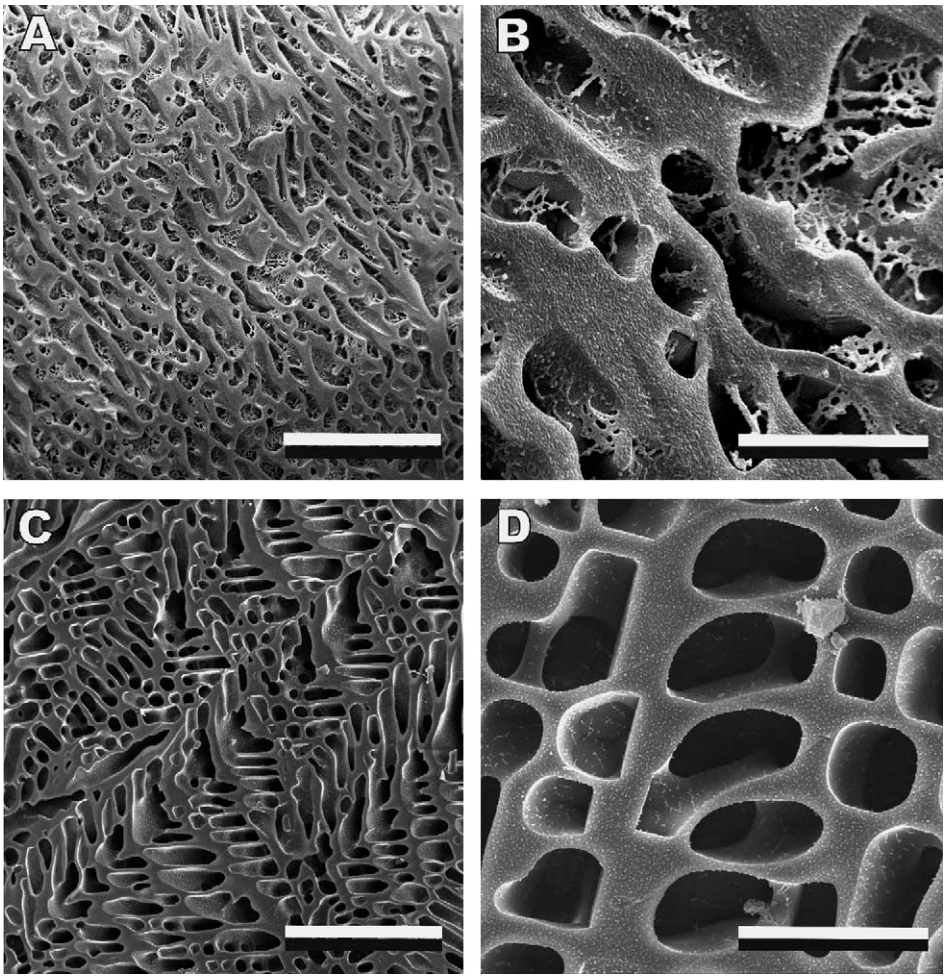

Fig. 6. Microstructure, as determined by cryo-SEM, of 40% sucrose solutions at −35 °C during the first warm (A and B) and during the second warm (C and D), following the same freezing protocol as for the images in Fig. 5. Bar = 100 μm in (A) and (C) and 15 μm in (B) and (D).

(Table 1). The midpoint temperature during warming was similar to the midpoint of the 40% sucrose solution at Tr_2.

4. Discussion

The two-cycle cooling and heating profile was used to create two different structures from the same sample to compare their thermal behavior and relate it to their structure as examined microscopically. The structure in the first cool cycle was developed by quiescent freezing: deep undercooling (to about −20 °C) followed by rapid nucleation. Annealing was conducted to promote maximal freeze-concentration. Then this structure was warmed to determine the thermal properties resulting from such a freezing regime. Most, but not all, of the crystals were melted during the first warm. The remaining crystals were then allowed to grow slowly with no further nucleation (as observed by microscopy) during the second cool, to promote extensive recrystallization, and the thermal properties of the structure thus created were analyzed in the second warm.

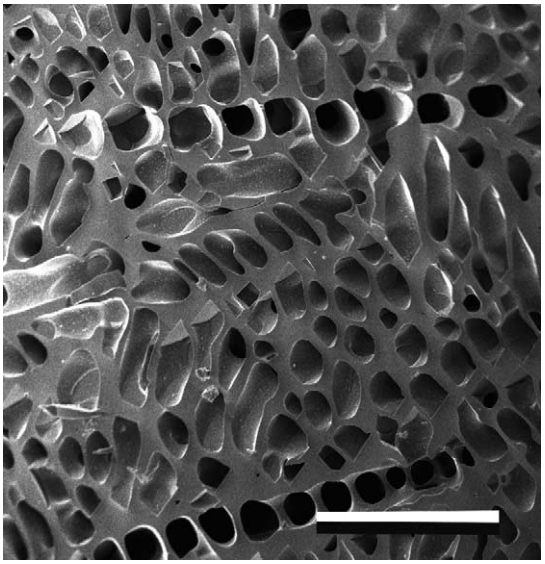

Fig. 7. Microstructure, as determined by cryo-SEM, of a 40% sucrose solution after cooling at 2 °C/min to −25 °C, warming at 2 °C/min to −10 °C, holding 20 min, cooling at 2 °C/min to −80 °C, annealing at −35 °C for 60 min, cooling to −80 °C and warming 2 °C/min to −35 °C. Bar = 60 μm.

The two-cycle temperature treatment resulted in thermal behavior similar to that seen earlier for the samples from the scraped-surface freezing process, from quiescently frozen and temperature cycled samples and from stored samples [16], viz. no Tr_2 in the reversing heat capacity curve in the second warm, although it was seen in the total heat flow curve. It would thus appear that the microstructure from rapidly nucleated crystals resulted in Tr_2 as a glass transition during warming, while a maturation of these crystals led to a loss of Tr_2 as a glass transition during the second warming cycle. Micrographs of the structure resulting from this freezing process have revealed the presence of sucrose inclusions within the ice crystals themselves. Although the size and morphology of the crystals would also be expected to differ from these freezing processes (and did, see Fig. 6), the presence of solute inclusions is perhaps the most important difference between the structures. It may be that the presence of solute inclusions in the ice crystals led to sufficient light scattering in the light microscope that ice crystals could not be resolved from the first cool or the first warm until −15 °C. Chen et al. [22] showed a direct correlation between

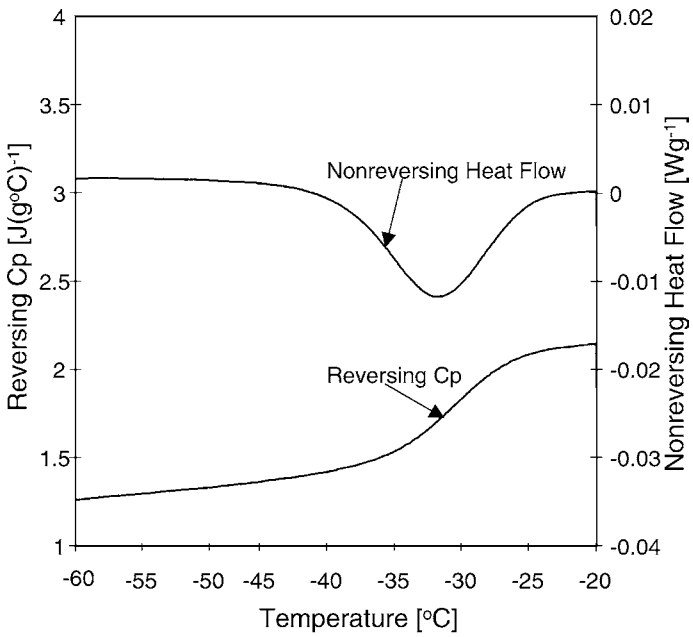

Fig. 8. Reversing heat capacity and non-reversing heat flow as a function of temperature for an 82% sucrose solution.

ice growth rate and impurities entrained in the ice during the freezing of 20–30% sucrose solutions. In the two cooling cycles reported here, one would expect large differences in ice growth rates.

It should be possible to ascribe the physical phenomena occurring within the sample during these temperature cycles to a state diagram. Fig. 9 presents an attempt to do this. During the first cool of the two-cycle process, crystallization is so rapid and heterogeneous that solutes are trapped within the structure of the growing crystals, as seen in Fig. 6. As a result of this system fractionation, the first cooling sweep can be modeled on the state diagram as paths a, b, c, d, representing non-equilibrium freezing of the solution, and paths a, b, e, f, representing vitrification of the plasticized solutes within the crystals. Point e would be the Tr_2 on cooling, as the plasticized solutes within the crystals hit the glass transition line. Point c would be the Tr_1 on cooling, as the bulk phase hits the glass transition line. The system was then annealed, which could be modeled as paths d, c, g, h. During this process, the bulk phase is maximally freeze-concentrated, with formation of more ice (T_g midpoint of $-45.9\,^{\circ}C$ increased to T_g' midpoint of $-43.4\,^{\circ}C$ in total heat flow, Table 1). Since there is less sucrose in the bulk phase, as a result of fractionation, more ice would form on freezing, and the system would still achieve maximal freeze-concentration (~82% sucrose) in the unfrozen phase at T_g'.

Paths h, g, i, b, a in Fig. 9 represents the warming of the bulk phase in the first warm. The bulk phase crosses the glass transition line at point g, appearing as the Tr_1, and since the system is maximally freeze-concentrated, this represents the T_g' of the system. The system warms from point g to i with no melting of ice, due to the high viscosity of the bulk phase and the kinetics of water dissolution into it. Thus, point i represents the T_m' of the system, the delayed onset of melting. The plasticized solutes would follow paths f, e, i, b, a. Point e would represent a glass transition, appearing as Tr_2 in the total and reversing heat flow curves in the second warm. As soon as this phase devitrifies and the crystal begins to melt, the two paths would quickly converge at, or slightly above, point i. The events at point i and e are concurrent in the Tr_2. This fractionation thus explains the appearance of a reversing heat flow (and total heat flow) Tr_2 during the first cool and a reversing Tr_2 during the first warm.

The second cool occurs slowly with extensive recrystallization, thus solutes are voided from the surface of the growing, pure ice crystal (Fig. 6). This process is modeled by paths a, b, c, d in Fig. 9. In this case, there is no Tr_2 during cooling (Figs. 1 and 3) as there is neither a glass transition event nor a T_m'. There could not be the equivalent of a delayed onset of melting due to high viscosity [11,14,15] during the cooling process. If there is more glass in the system during the second cool than the first, this could account for a slightly larger height and lower temperature at Tr_1 (Table 1 and Fig. 3). At this point, the system is not maximally freeze-concentrated. During annealing, the system follows paths d, c, g, h, as further ice is formed (T_g midpoint of $-49.3\,^{\circ}C$ increased to T_g' midpoint of $-43.5\,^{\circ}C$ in total heat flow, Table 1).

On warming in the second cycle, the bulk, unfrozen phase devitrifies at point g, the T_g', which appears as the Tr_1 (Figs. 2 and 3). This is exactly the same as the Tr_1 in the first warm (Fig. 2). The 82% sucrose sample shows one broader baseline shift transition, all in the reversing curve (Fig. 7). The temperature is higher in the warming curve, after annealing, than the Tr_1 in the second warm. However, on a per weight of glass basis, the height of the 82% sucrose transition is exactly the same as the Tr_1 of the 40% sucrose solution (Tables 1 and 2). The delayed onset of melting at point i results in a T_m' in the total heat flow curve during the second warm (Fig. 2), but this is a first order process which does not show up in the reversing heat capacity curve (Fig. 3). It might be expected that if Tr_2 in the first warm is comprised of both the T_g of the solute inclusions and the T_m' of the bulk phase, it should be larger than the Tr_2 in the second warm, which is comprised of simply the latter. However, the devitrification overshoot (Fig. 2) makes it difficult to accurately quantify the height of the transition, and the differing quantities of bulk-phase glass in the system would give rise to different sizes of T_m'. The important point is that at the end of the complex relaxation and the beginning of the melting endotherm, the thermograms from both warming cycles converge (Fig. 2), meaning the total enthalpy of relaxation from beginning to end is the same, regardless of how it is partitioned.

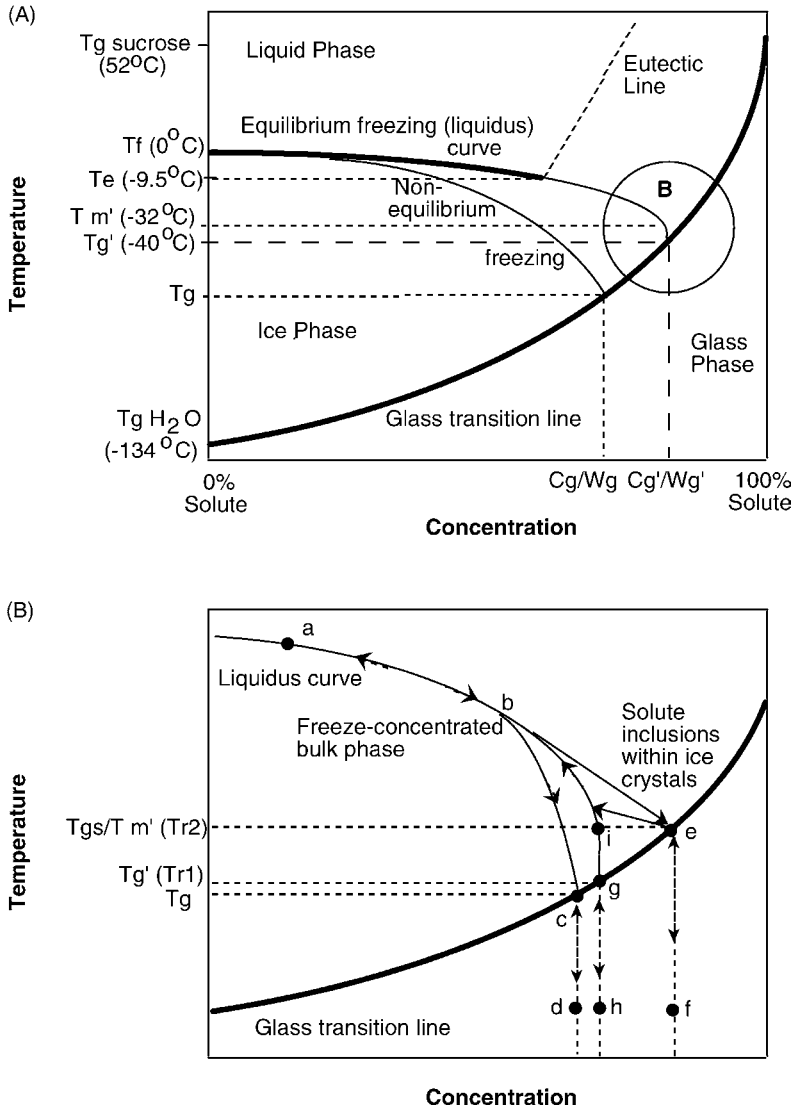

Fig. 9. (A) A schematic temperature-concentration state diagram for an aqueous carbohydrate solution, showing the glass transition curve, defined by viscosity, which extends from the T_g (glass transition temperature) of pure water (−134 °C) to the T_g of pure solute, the equilibrium freezing (liquidus) curve, which extends from the T_m (melting temperature) of pure water (0 °C) to the eutectic temperature (T_e) of the solute, and the theoretical eutectic line. The liquidus curve extends below T_e in a non-equilibrium state to intersect with the glass transition line at point T'_g, which represents the glass transition temperature of the maximally freeze-concentrated solution [8,9]. W'_g represents the amount of unfrozen water (100% solute, C'_g) that becomes trapped in the glass. Point T'_m reflects the temperature needed to cause mechanical collapse and ice melting to occur above the glass transition during warming [14,15]. Points T_g and W_g represent an example of a temperature concentration relationship in a glass formed as a result of less than maximal ice formation (following a "non-equilibrium" freezing line). (B) The region circled in A is expanded to show the processes occurring during the two-cycle cooling and heating protocol. Paths a, b, c, d and a, b, e, f represents the first cool, in which the system fractionates due to rapid nucleation and entrapment of solute inclusions within the ice crystals. Paths d, c, g, h represents the annealing process in the unfrozen phase. Paths h, g, i, b, a and f, e, i, b, a represent the first warm, in which the solute inclusions redissolve. Paths a, b, c, d represents the second cool, in which slow freezing has prevented solute inclusion. Paths d, c, g, h represents the second anneal. Paths h, g, i, b, a represents the second warm.

The tempering protocol produced the same results as the second warm of the two-cycle protocol, simply because after the system was allowed to nucleate, those nuclei were then allowed to grow under slow conditions where pure ice crystals would be expected (Fig. 8). This reconciles what appeared to be a contradiction in the literature between the MT–DSC results of Aubuchon et al. [13] and those of Knopp et al. [18]. Aubuchon et al. [13] concluded that Tr_2 is a glass transition (or at least appears glass transition-like). However, they followed a "slow freeze and anneal" method and thus would have ended up with the same structure as we have shown for the first warm of the two-cycle protocol, viz. solute inclusions from rapid nucleation following deep undercooling. Knopp et al. [18] concluded that Tr_2 was not a glass transition, but the onset of melting. They used the tempering method and thus would have ended up with crystals that had matured and perfected, thus eliminating any potential for solute inclusion.

5. Conclusions

Freezing protocol was seen to have a large impact on both sample microstructure and thermal behavior in frozen sucrose solutions. Deep undercooling followed by rapid nucleation and continual lowering of the temperature led to a system that showed solute inclusions within the ice crystals themselves. These solute inclusions led to a complex relaxation in which both the bulk phase and the plasticized solutes underwent a glass transition, leading to what looked like a double glass transition. On the other hand, the presence of a small number of ice nuclei at high temperature followed by a slow growth of these nuclei led to pure ice crystals and a homogeneous bulk phase in which only one glass transition was seen.

Acknowledgements

Financial support from the Natural Sciences and Engineering Research Council of Canada was gratefully received.

References

[1] H.D. Goff, Food Res. Int. 25 (1992) 317.
[2] G. Blond, D. Simatos, Thermochim. Acta 175 (1991) 239.
[3] S. Ablett, M.J. Izzard, P.J. Lillford, J. Chem. Soc., Faraday Trans. 88 (1992) 789.
[4] M. Le Meste, V. Huang, J. Food Sci. 57 (1992) 1230.
[5] W.M. MacInnes, The glassy state in foods, in: J.M.V. Blanshard, P.J. Lillford (Eds.), Nottingham University Press, Loughborough, UK, 1993, p. 223.
[6] M.E. Sahagian, H.D. Goff, Thermochim. Acta 246 (1994) 271.
[7] H.D. Goff, M.E. Sahagian, Thermochim. Acta 280 (1996) 449.
[8] H. Levine, L. Slade, J. Chem. Soc., Faraday Trans. I 84 (1988) 2619.
[9] H. Levine, L. Slade, Cryo-Lett. 9 (1988) 21.
[10] Y. Roos, M. Karel, Int. J. Food Sci. Technol. 26 (1991) 553.
[11] S. Ablett, A.H. Clark, M.J. Izzard, P.J. Lillford, J. Chem. Soc., Faraday Trans. 88 (1992) 795.
[12] H.D. Goff, Pure Appl. Chem. 67 (1995) 1801.
[13] S.R. Aubuchon, L.C. Thomas, W. Theuerl, H. Renner, J. Thermal Anal. 52 (1998) 53.
[14] E.Y. Shalaev, F. Franks, J. Chem. Soc., Faraday Trans. 91 (1995) 1511.
[15] W.Q. Sun, Cryo-Lett. 18 (1997) 99.
[16] H.D. Goff, K. Montoya, M.E. Sahagian, in: H. Levine (Eds.), Progress in Amorphous Food and Pharmaceutical Systems, Royal Society of Chemistry, London, in press.
[17] M.J. Izzard, S. Ablett, P.J. Lillford, V.L. Hill, I.F. Groves, J. Thermal Anal. 47 (1996) 1407.
[18] S.A. Knopp, C. Chongprasert, S.L. Nail, J. Thermal Anal. 54 (1998) 659.
[19] K.B. Caldwell, H.D. Goff, D.W. Stanley, Food Struct. 11 (1992) 1.
[20] A.A. Flores, H.D. Goff, J. Dairy Sci. 82 (1999) 1399.
[21] R.H.M. Hatley, C. van den Berg, F. Franks, Cryo-Lett. 12 (1991) 113.
[22] P. Chen, X.D. Chen, K.W. Free, J. Food Eng. 38 (1998) 1.